Surface Modulation via Conjugated Bithiophene Ammonium Salt for Efficient Inverted Perovskite Solar Cells

Xin Zhang[abcdef], Stijn Eurelings[g], Andrea Bracesco[g], Wenya Song[cdef], Stijn Lenaers[f], Wouter Van Gompel[f], Anurag Krishna[def], Tom Aernouts[def], Laurence Lutsen[ef], Dirk Vanderzande[ef], Mariadriana Creatore[gh], Yiqiang Zhan[ab*], Yinghuan Kuang[def*] and Jef Poortmans[cdef]

[*]Corresponding authors: yqzhan@fudan.edu.cn;Yinghuan.Kuang@imec.be

[a]Center for Micro Nano Systems, School of Information Science and Technology (SIST), Fudan University, Handan 220, Shanghai, 200433, China

[b]Academy for Engineering & Technology (FAET), Fudan University, Handan 220, Shanghai, 200433, China

[c]Department of Electrical Engineering (ESAT), KU Leuven, Kasteelpark Arenberg 10, Leuven, 3001, Belgium

[d]Imec, imo-imomec, Thin Film PV Technology – partner in Solliance, Thor Park 8320, Genk, 3600, Belgium

[e]EnergyVille, imo-imomec, Thor Park 8320, Genk, 3600, Belgium

[f]Hasselt University, imo-imomec, Martelarenlaan 42, Hasselt, 3500, Belgium

[g]Plasma & Materials Processing, Department of Applied Physics and Science of Education, Eindhoven University of Technology (TU/e), P.O. Box 513, 5600 MB Eindhoven, The Netherlands

[h]Eindhoven Institute of Renewable Energy Systems (EIRES), 5600 MB Eindhoven, The Netherlands

Abstract

The metal halide perovskite absorbers are prone to surface defects which severely limit the power conversion efficiencies (PCEs) and the operational stability of the perovskite solar cells (PSCs). Herein, trace amounts of bithiophenepropylammonium iodide (bi-TPAI) are applied to modulate the surface properties of the gas-quenched perovskite. It is found that the bi-TPAI surface treatment has negligible impact on the perovskite morphology, but it can induce a defect passivation effect and facilitate the charge carrier extraction, contributing to the gain in the open-circuit voltage (V_{oc}) and fill factor (FF). As a result, the PCE of the gas-quenched sputtered NiO_x-based inverted PSCs is enhanced from the initial 20.0% to 22.0%. Most importantly, the bi-TPAI treatment can largely alleviate or even eliminate the burn-in process during the maximum power point tracking (MPPT) measurement, improving the operational stability of the devices.

1. Introduction

The inverted p-i-n perovskite solar cells (PSCs) have gained huge attention due to their sky-rocketed power conversion efficiencies (PCEs) with achieving the certified record of 25.4%.[1] During the past few years, the quality of perovskite films has been largely improved due to the advances made in film processing via compositional and additive engineering,[2-6] which partly contributes to the rapid development in PCEs. Moreover, since the interfaces between perovskite and charge transport layers are now considered to be the main limiting factors that hinder the further gain in the device efficiency and operational stability,[7-11] interface engineering is generally applied in the highly efficient inverted PSCs.

Notably, among the hole transport layers (HTL) that are used in the inverted PSCs,[12-19] nickel oxide (NiO_x) prepared by magnetron sputtering is eye-catching due to its unique properties of scalability, high deposition throughput, robust reproducibility, low-cost and the facile control over the process, which match the requirements of the upscaling of perovskite photovoltaics. However, the performance of sputtered NiO_x-based PSCs is still lagging behind those counterparts employing well-studied organic HTLs such as Poly[bis(4-phenyl)(2,4,6-

trimethylphenyl)amine] (PTAA). For instance, the PTAA based inverted PSCs can reach a PCE >24%,[20] while the poor wettability of perovskite precursor on PTAA hinder its application in large-area devices. Consequently, it is worthwhile to make efforts to improve the device performance of the sputtered NiO_x based PSCs. On the one hand, a redox-reaction-induced hole extraction barrier and mismatched band alignment at the NiO_x/perovskite interface constrain the acquisition of a high open-circuit voltage (V_{oc}),[21] which can be addressed by introducing thin self-assembled monolayers (SAMs) as reported previously.[22-24] On the other hand, the perovskite surface has been known to contain defects and mobile ions, which are detrimental to both performance and operational stability. In particular, during the operational stability tests, the devices are known to exhibit a rapid loss in PCE which is termed as "burn-in" effect.[25, 26] It has been reported that defect-mediated ion migration leads to ion aggregation at the top interface, which inhibits the efficient extraction of carriers, and results in burn-in behavior under operational conditions.[27] As a result, numerous surface modification strategies have been developed to passivate surface defects.[28] Recently, Jiang *et al.* adopted a reactive surface engineering approach to reduce the surface potential fluctuations and suppress the formation of iodine vacancies, thus realizing a PCE of exceeding 25% for the inverted PSCs.[29] Nevertheless, previous studies regarding the sputtered NiO_x-based inverted PSCs were mainly focused on the buried HTL/perovskite interface with improving the PCEs to nearby 20%,[30-34] which are backward. Therefore, more research on perovskite surface treatment is required to accelerate the development of the inverted PSCs based on sputtered NiO_x, thus faster commericallization.

In this work, we simultaneously upgrade the two interfaces adjacent to the perovskite layer in order to maximize the gain in the device performance. Firstly, SAMs are introduced to modify the sputtered NiO_x. More importantly, a conjugated organic ammonium salt, i.e., bithiophenepropylammonium iodide (bi-TPAI), is employed to improve the top surface properties of gas-quenched CsFA double cation perovskite. Through the analysis of the surface elemental compositions and the surface morphology, it can be found that bi-TPAI is effectively retained on the surface of perovskite without affecting the surface morphology. With the bi-TPAI surface modulation, the steady-state photoluminescence (PL) intensity increases, and the carrier lifetime extends, indicating the reduction of the surface defects. In addition, the build-in voltage (V_{bi}) of the device boosts from the initial 1.05 V to 1.11 V, and a faster carrier extraction process is observed. Consequently, the gas-quenched inverted PSCs deliver the highest PCE of 22.0%, whereas the control device possesses 20.0%, mainly attributing to the

improved V_{oc} and FF. Most importantly, the bi-TPAI surface modulation can largely alleviate or even eliminate the burn-in process during maximum power point tracking (MPPT) measurements, leading to stable operational behaviors of the PSCs.

2. Experimental section

2.1. Materials

Indium tin oxide (ITO) coated glass substrates were purchased from Colorado Concept Coatings LLC. Methylammonium chloride (MACl, 99.99%) and Formamidinium iodide (FAI, 99.99%) were purchased from Greatcell Solar Materials. Lead iodide (PbI_2, 99.99%), [4-(3,6-Dimethyl-9H-carbazol-9-yl)butyl]phosphonic acid (Me-4PACz, 99.0%) and cesium iodide (CsI, 99.0%) were purchased from Tokyo Chemical Industry (TCI). Lead bromide ($PbBr_2$, 99.999%), acetonitrile (99.8%), 4-tert-butylpyridine (4-tBP, 98%), bis (trifluoromethylsulfonyl)-imide lithium salt (Li-TFSI, 99.99%), tris(2-(1Hpyrazol-1-yl)-4-tert-butylpyridine) cobalt(III) tri[bis(trifluoromethane) sulfonimide] (FK 209; Co(III) TFSI salt, 98%), lithium fluoride (LiF, 99.99%), chlorobenzene (99.8%), anhydrous dimethylformamide (DMF, 99.8%), anhydrous 1-methyl-2-pyrrolidone (NMP, 99.5%) and anhydrous isopropanol alcohol (IPA, 99.5%) were purchased from Sigma Aldrich. Fullerene C_{60} (99.95%) was purchased from Nano-C. Bathocuproine (BCP, 99.5%) was purchased from Luminescence Technology Corp. (Lumtec). Absolute acetone (99.5%) and isopropanol (98%) were purchased from VWR. 2,2',7,7'-tetrakis(N,N-di-p-methoxyphenyl-amine)9,9'-spirobifluorene (spiro-OMeTAD, 99.5%) was purchased from Xi'an Polymer Light Technology Corp. All materials were used as received. The bi-TPAI was synthesized as described in a previous publication by some of the authors where a fundamental study into the formation of two-dimensional (2D) perovskites using bithiophene derivatives was performed.[35]

2.2. Device fabrication

Indium tin oxide (ITO) coated substrates (15 Ω sq^{-1}) of 3 cm × 3 cm were ultrasonic cleaned in diluted detergent, deionized water, acetone and isopropanol for 15 minutes, respectively. Then the substrates were dried in air in a fume hood and transferred to a nitrogen-filled glove box. A 15 nm thick NiO_x film was deposited on the substrate by reactive direct-current (DC) sputtering from a metallic nickel target in oxygen plasma at 3 mTorr pressure. The as-prepared NiO_x film was then annealed at 300 °C for 20 min in air with relative humidity of ~40-50%. The 1.35 M dual cation perovskite ($Cs_{0.1}FA_{0.9}PbI_{2.855}Br_{0.145}$) precursor was prepared by dissolving 70.2 mg CsI, 418 mg FAI, 1154 mg PbI_2 and 71.8 mg $PbBr_2$ in 2.0 mL

DMF/NMP (9:1 vol:vol) mixed solvent. 30 mol% of MACl was used as additive in the precursor. Before using, the perovskite precursor was diluted from 1.35 M to 1.1 M. Then, it was dynamically spin-coated on the substrates by a continuous two-step program, which is 2000 rpm for 10 s and then 5000 rpm for 45 seconds. During this process, the perovskite film was quenched with nitrogen for 30 s, starting at 40 seconds prior to the end. Then the perovskite films were annealed at 110 °C for 70 minutes. For the bi-TPAI treatment, different concentrations of bi-TPAI were spin-coated on top of the perovskite films, followed by annealing at 110 °C for 5 min. Afterwards, the samples were transferred into a high-vacuum chamber with the base pressure of $10^{-7} \sim 10^{-8}$ Torr to deposit 0.8 nm LiF, 20 nm C_{60} (0.5 Å/s) and 5 nm BCP (0.5 Å/s) by thermal evaporation. A 100 nm thick copper (Cu) layer was prepared by thermal evaporation at 2 Å/s rate. Finally, A 100 nm thick MgF_2 layer was thermally evaporated at 2 Å/s rate on the glass side. The active cell area of 0.13 cm^2 is defined by a metal mask. For the hole-only devices, spiro-OMeTAD solution in chlorobenzene (72.3 mg/mL) with dpoing 18 μL Li-TFSI (520 mg/mL in acetonitrile), 25 μL of FK209 (300 mg/mL in acetonitrile), and 29 μL of 4-tBP was dynamiclly spin-coated at 3000 rpm for 30 s, then a 85 nm thick gold (Au) layer was prepared by thermal evaporation at 0.5 Å/s rate.

2.3. Characterizations

The current-voltage (*J-V*) characteristics and maximum power point tracking (MPPT) were measured without any pre-conditioning in an N_2 filled glove box at 30 °C, using Abet Sun 3000 solar simulator. A Keithley 2602A source meter was used to record the *I-V* of the PSCs (1 V s^{-1}, 10 mV step). The simulated solar irradiation of 100 mW cm^{-2} was obtained from a 450 W xenon lamp, which was calibrated with a Fraunhofer ISE's WPVS reference solar cell (Type: RS-ID-4). The maximum power point tracking was recorded following our previous work, which is a dynamic tracking process.[36] The top-view SEM images of the perovskite films were obtained by a field-emission SEM under an accelerating voltage of 5 kV (Nova 200, FEI). The dark *J-V* curves, C-V, C-f, TPC and TPV were characterized using PAIOS from FLUXiM. UV-Vis absorption spectra were obtained using a UV-1601PC spectrophotometer (Shimadzu). The steady-state and time-resolved PL measurements were performed on PicoQuant FluoTime 300 in ambient. XRD was measured by Bruker D8 diffractometer equipped with Cu-Kα X-rays (λ = 1,5418 Å). The diffractograms were measured in the range of 10°–60° with step size of 0.04°. The surface composition of the perovskite is investigated by means of XPS in a Thermo Scientific K-Alpha system, equipped with an Al Kα x-ray source (1487 eV) without any presputtering. Using THERMO AVANTAGE software, each spectral feature is fitted with

Gaussian/Lorentzian mixed peaks, which have a fixed full width half maximum for each chemical state across all the pristine perovskite and bi-TPAI treated samples. For each sample, unless specified otherwise, the binding energies (BE) of the spectral features are aligned such that the perovskite C1s spectral feature occurs at 284.8 eV.

3. Results and discussion

Figure 1a shows the chemical structure of bi-TPAI, and the device architecture used in this work is MgF_2/ITO/sputtered NiO_x/Me-4PACz/perovskite/bi-TPAI/LiF/C_{60}/BCP/Cu. The optimum bi-TPAI concentration, which is 0.01 mg/mL, is determined from a screening experiment (**Figure S1**), and the PSCs under different conditions show small hysteresis (**Figure S2**). **Figure 1b** shows the current density-voltage (*J-V*) curves for the best control and bi-TPAI treated PSCs. The control device shows short-circuit current density (J_{sc}), V_{oc}, and fill factor (FF) of 24.5 mA cm^{-2}, 1.08 V, and 75.4%, respectively, giving a PCE of 20.0%. After the bi-TPAI treatment, V_{oc} and FF are significantly improved, resulting in an enhanced PCE of 22.0%, with J_{sc}, V_{oc}, and FF of 24.6 mA cm^{-2}, 1.12 V, and 79.8%, respectively. To the best of our knowledge, this is one of the highest reported PCEs for the inverted p-i-n PSCs using sputtered NiO_x as HTL (**Figure S3** and **Table S1**). The external quantum efficiency (EQE) spectra of both control and bis-TAPI treated PSCs show only negligible differences (**Figure 1c**), which agrees with the subtle changes in J_{sc} as determined by *J-V* scans. The integrated values from EQE match well with the *J-V* scans as the relative differences are within 3% in both cases. As shown in **Figure 1d**, during the 10 min MPPT measurements, the stabilized PCE is improved from ~18% to ~21% after the bi-TPAI treatment. It should be noted that the burn-in loss is also noticeably reduced. As shown in **Figure S4**, the burn-in behavior of the PSCs is gradually eliminated by further increasing the bi-TPAI concentration, while a too-high concentration of bi-TPAI modification results in a decreased initial PCE. This is because too-high concentration of bi-TPAI could result in the excess bi-TPA^{+} cations on the surface, which hinders the charge extraction at the perovskite/C_{60} interface, thus decreased FF and J_{sc} (**Figure S1**). In addition, PSCs with pure IPA treatment (the solvent in which bi-TPAI is dissolved) and with the additional 5 min perovskite post-annealing (to compare the effect of the extra annealing) are fabricated as additional control devices, respectively. As shown in **Figure S5**, PSCs prepared under these conditions show comparable PCEs and MPPT behavior to the control device. Therefore, IPA and the additional annealing time are not responsible for the improved and tunable MPPT PCEs, rather this phenomenon is originating from the introduction of the bi-TPAI on the perovskite surface. **Figure 1e** shows the statistical diagram

of the PCE for the control and the bi-TPAI treated PSCs. The detailed results are summarized in **Table 1**. With the bi-TPAI treatment, the average PCE is improved from 19.0% to 20.5%, mainly due to enhanced V_{oc}, indicating that the bi-TPAI treatment could passivate the surface defects.
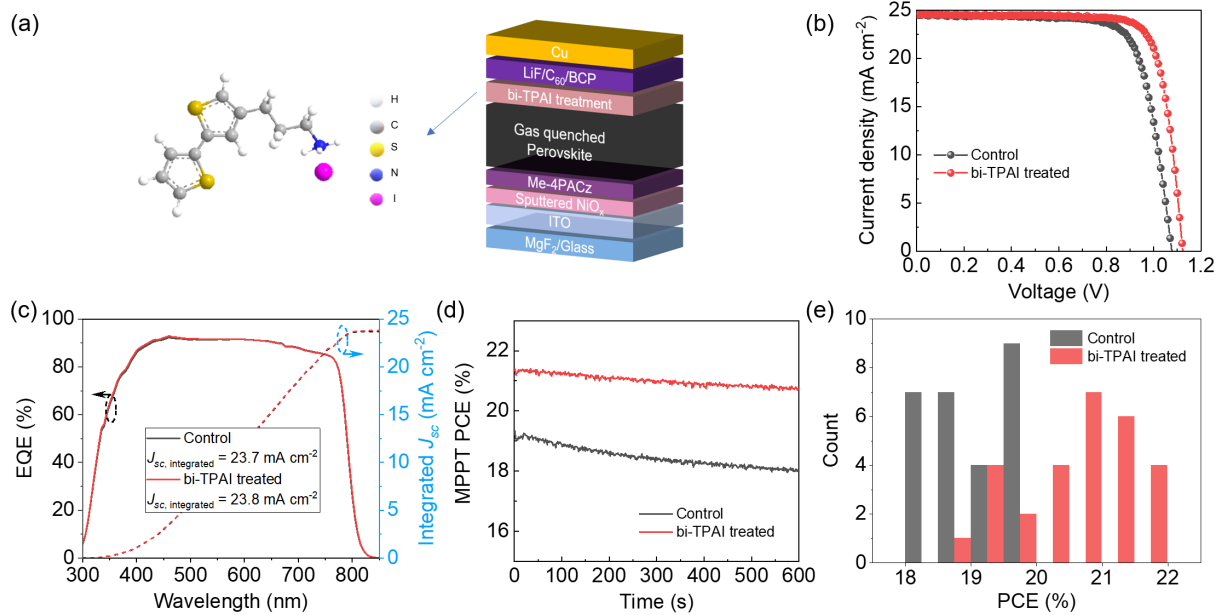

Figure 1. (a) The chemical structure of bi-TPAI and the device architecture of the gas-quenched inverted PSCs. (b) *J-V* curves of the best control and bi-TPAI treated PSCs. (c) EQE spectra, (d) 10 min MPPT measurement, and (e) statistical diagram of PCE for the control and the bi-TPAI treated PSCs.

Table 1. Average photovoltaic parameters of the control and the bi-TPAI treated PSCs. 27 and 28 devices are counted respectively for the control and the bi-TPAI treated PSCs. Results are expressed as mean value ± standard deviation.

	J_{sc} (mA/cm^2)	V_{oc} (V)	FF (%)	PCE (%)
Control	24.0 ± 0.4	1.08 ± 0.01	73.1 ± 2.1	19.0 ± 0.6
bi-TPAI treated	24.3 ± 0.3	1.12 ± 0.01	75.3 ± 2.9	20.5 ± 0.8

To understand the effect of the bi-TPAI surface treatment, X-ray photoelectron spectroscopy (XPS) measurements are performed to study the elemental properties of the perovskite surface under different conditions. **Figure 2a-e** shows the C1s spectra of the corresponding perovskite films treated by different concentrations of bi-TPAI. Overall, the core level peaks of C1s consist of three components. For the control perovskite film (**Figure 2a**), the peak located at the highest binding energy position of ~288.3 eV is assigned to the C=NH$_2$ bonds from the FA$^+$ cations. The one located in the middle has a position of ~286.4 eV, which belongs to the C-NH$_2$ species. The peak located at the lowest binding energy of ~284.8

eV is attributed to C-C or C-H bonds.[37] With increasing the concentration of bi-TPAI, the intensity of the C-C and C-NH$_2$ peaks changes, and the ratio of their integrated areas gradually increases (**Figure S6**). This suggests that, as expected, more bi-TPAI is retained on the surface of the perovskite with increasing its concentration, since bi-TPAI contains relatively more C-C bonds. Meanwhile, bi-TPAI contains C-S bonds, which shift the peak at ~286.4 eV towards a lower binding energy position. **Figure 2f** shows the S2p XPS spectra of the corresponding perovskite films. No signal belonging to the sulfur is observed for the control and for the 0.01 mg/mL bi-TPAI treated perovskite films. A weak signal is observed for a sample treated with 0.05 mg/mL of bi-TPAI and becomes more pronounced with increasing concentration thereafter, indicating that bi-TPAI is indeed present on the surface of the perovskite films. Notably, the peak in the middle position is found to shift from ~286.4 eV to ~286.0 eV even under 0.01 mg/mL of bi-TPAI in the C1s XPS spectra (**Figure 2a** and **b**), and the (C-C)/(C=NH$_2$) peak area ratio increases slightly (**Figure S6**), suggesting that even low concentrations of bi-TPAI introduces bi-TPA$^+$ to form at the film surface. We further obtain the Pb4f XPS spectra of the perovskite films. As shown in **Figure S7**, the peaks located at 138.4 eV and 143.2 eV in the control perovskite film are assigned to Pb 4f$_{7/2}$ and Pb 4f$_{5/2}$, respectively. With the bi-TPAI treatment, these peaks shift to lower binding energy positions of 138.0 eV and 142.9 eV, respectively. This indicates an interaction between the bi-TPA$^+$ and Pb^{2+}, which could passivate the surface Pb^{2+}-related defects.
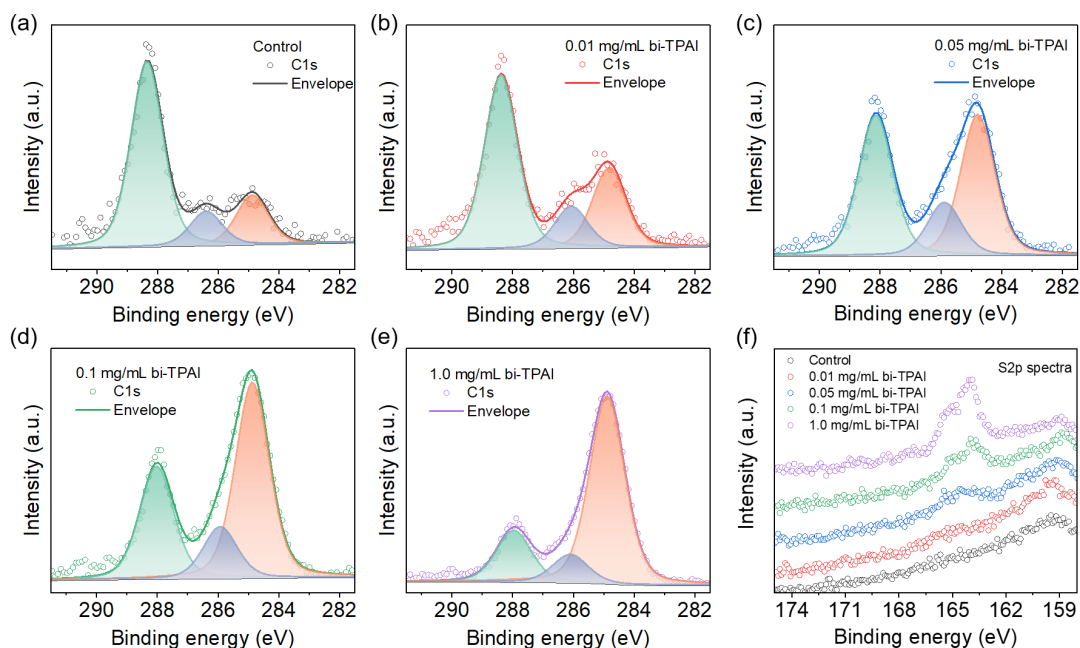

Figure 2. C1s XPS spectra of the perovskite films under (a) no bi-TPAI treatment (control), (b) 0.01 mg/mL bi-TPAI (as bi-TPAI treated in the text), (c) 0.05 mg/mL bi-TPAI, (d) 0.1 mg/mL bi-TPAI and (e) 1.0 mg/mL bi-TPAI conditions. (f) S2p XPS spectra of the corresponding perovskite films.

Next, we study the effect of bi-TPAI treatment on the perovskite film morphology by scanning electron microscopy (SEM). As shown in **Figure 3a** and **b**, pinhole-free compact perovskite films consisting of large grains are observed for both conditions, indicating that the bi-TPAI treatment has a negligible effect on the grain size and the film morphology. In addition, the bi-TPAI treatment also does not affect the optical absorption of the perovskite films, as the absorption spectra are practically identical (**Figure 3c**). The absorption onsets of both conditions are identical, which indicates that the band gap of the perovskite remains unchanged. This can be supported by the identical Tauc plots for all of the perovskite films (**Figure S8**). The effect of the bi-TPAI treatment on the perovskite crystal structure is studied by X-ray diffraction (XRD). As displayed in **Figure 3d**, both perovskite films show two main diffraction peaks of ~14.0° and ~28.2°, corresponding to the (001) and (002) planes of cubic-phase perovskite.[38] It should be noted that 2D perovskite is not formed after the bi-TPAI treatment, since there is no additional reflections for the treated film at lower 2 theta regions (**Figure S9**). Steady-state PL and time-resolved PL are performed to further investigate the carrier dynamics of the perovskite films. As shown in **Figure 3e**, both perovskite films show identical PL peak positions, while the peak intensity is enhanced with the bi-TPAI treatment. In addition, the average carrier lifetime is calculated based on the following equations,

$$I(t) = A_1 \exp\left(-\frac{t}{\tau_1}\right) + A_2 \exp\left(-\frac{t}{\tau_2}\right), \qquad (1)$$

$$\tau_{average} = \frac{A_1\tau_1^2 + A_2\tau_2^2}{A_1\tau_1 + A_2\tau_2}, \qquad (2)$$

where τ_1 is fast-decay carrier lifetime and τ_2 is the slow-decay carrier lifetime. The average carrier lifetime increases from 271 ns for the control film to 445 ns for the bi-TPAI treated film (**Table S2**). These results suggest that fewer defects are present after the bi-TPAI treatment, which is expected to be beneficial for the V_{oc} of the PSCs.
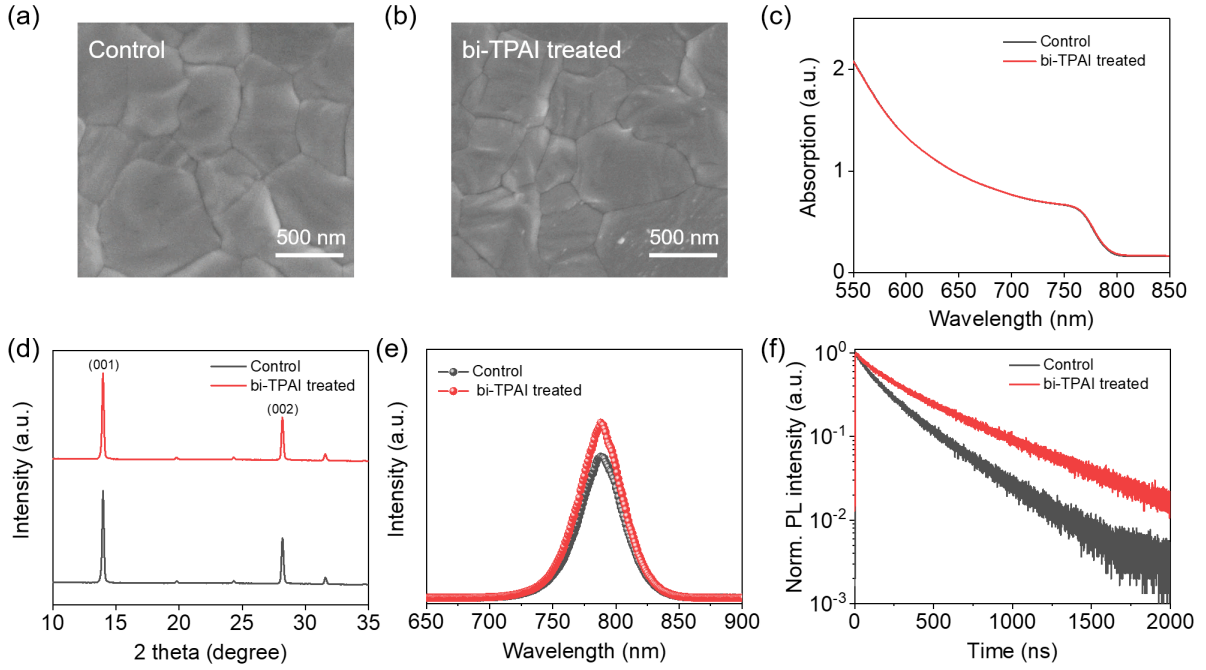
Figure 3. Top-view SEM images of (a) control and (b) bi-TPAI treated perovskite films. (c) UV-Vis absorption spectra, (d) XRD patterns, (e) steady-state PL, and (f) TRPL spectra of the perovskite films deposited on ITO/sputtered NiO_x/Me-4PACz substrates.

Next, *J-V* curves are acquired under dark conditions for the control and the bi-TPAI treated PSCs. As shown in **Figure 4a**, both devices show a similar dark current density under forward bias, but the bi-TPAI treated device has a lower dark current density at reverse bias. We further fit the curves using a single-diode model to acquire the information of ideality factor (*n*) and the series resistance of the PSCs. The series resistance is decreased from 6.01 $\Omega \cdot cm^2$ to 4.33 $\Omega \cdot cm^2$ after the bi-TPAI treatment, which is beneficial for enhancing the FF.[39] The *n* value is extracted to be 1.9 for the control device, while the bi-TPAI treated device has an ideality factor of 1.7. To further acquire the changes in *n* when the devices are under illumination, light-dependent V_{oc} measurements are performed for the control and bi-TPAI treated PSCs. **Figure 4b** shows the semilogarithmic plot of the corresponding results. Through fitting the V_{oc} with a slope of *nkT/q* (*k* is the Boltzmann's constant, *T* is the temperature in Kelvin, and *q* is the elementary charge), the *n* value is found to reduce from the initial 1.81 for the control device to 1.38 for the bi-TPAI treated device. The reduced *n* in both dark and illumination conditions indicates that trap-assisted recombination is suppressed.[40] Furthermore, space-charge-limited current measurements are conducted on the hole-only devices. As shown in **Figure 4c**, the trap-filled-limited voltage (V_{TFL}) for the control and the bi-TPAI devices are 0.38 V and 0.19 V, respectively. According to the equation of $N_t = 2\varepsilon_0 \varepsilon_r V_{TFL}/qL^2$ (ε_0 is the vacuum permittivity, ε_r is the dielectric constant of perovskite, *q* is the elementary charge, *L* is

the thickness of the perovskite), the N_t decreases from 7.89×10^{15} cm^{-3} to 3.94×10^{15} cm^{-3} after the bi-TPAI surface treatment. These results show a passivation effect of the bi-TPAI surface treatment. Mott-Schottky analysis is performed to understand the effect of bi-TPAI treatment on the built-in potential (V_{bi}). Capacitance-voltage measurements are carried out at 300 K at a fixed frequency of 1 kHz, which is determined from the capacitance-frequency measurement (**Figure S10**). As shown in **Figure 4d**, the V_{bi} of the control device is 1.05 V, whereas it is 1.11 V for the bi-TPAI treated device. The larger V_{bi} could also result in effective charge extraction to increase the V_{oc} and FF.[41, 42] To prove this hypothesis, transient photocurrent (TPC) and transient photovoltage (TPV) measurements are performed, as shown in **Figure 4e** and **f**. The TPC decay time for the control device is 1.60 µs. With the bi-TPAI treatment, the decay time decreases to 0.96 µs, indicating a superior charge carrier extraction process,[43] which is consistent with our hypothesis that larger V_{bi} would be beneficial to charge extraction. Furthermore, the TPV decay time of the bi-TPAI treated device is 16.5 µs, which is larger than that of the control device. This suggests that the bi-TPAI treated device has lower non-radiative recombination, resulting in higher V_{oc}.[44] Through the analysis above, we can deduce that the device performance enhancement originates from the combination of effective defect passivation, reduced series resistance, enlarged V_{bi}, and improved charge carrier extraction.
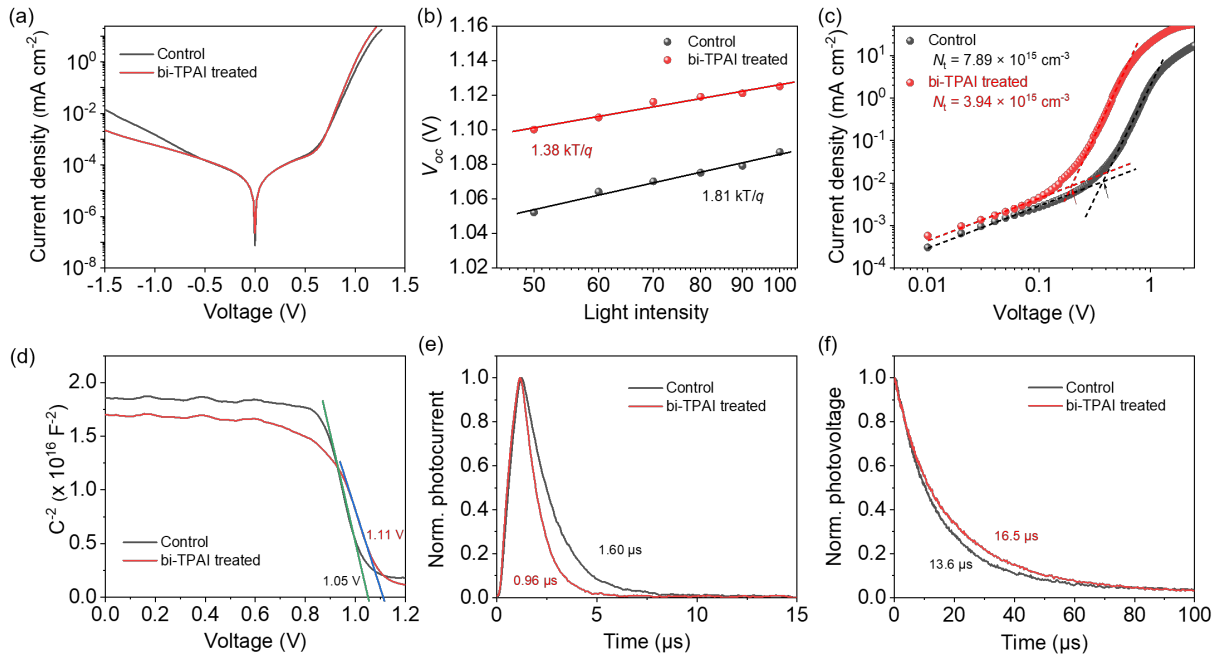

Figure 4. (a) *J-V* curves under dark conditions, (b) light-dependent V_{oc} measurements of the control and the bi-TPAI treated devices. (c) *J-V* curves of the hole-only devices under dark conditions. The device architecture is ITO/NiO$_x$/SAMs/perovskite/spiro-OMeTAD/Au. (d) Mott-Schottky plots, (e) TPC, and (f) TPV of the control and the bi-TPAI treated devices.

Stable operational behavior is extremely important for PSCs. We observe an improvement in MPPT PCE after the bi-TPAI treatment, which enables reduced density of defects and efficient carrier extraction. To better understand the effect of bi-TPAI on the device operational stability, a 1-hour MPPT measurement was further performed based on 3 different samples, specifically (1) the control device: lower efficiency and unstable MPPT, (2) the bi-TPAI (0.01 mg/mL) treated device: highest efficiency and moderately improved MPPT stability, and (3) the higher concentration bi-TPAI (0.1 mg/mL) modified device: comparable initial efficiency and the most stable MPPT. **Figure 5a** shows the normalized V_{mpp} for the corresponding devices. It is clear that the control device suffers from a fast burn-in process during the initial 15 min, after which the performance becomes stable over the time of the measurement. The bi-TPAI modified device exhibits a reduced burn-in phase and then stabilizes, while the device with increased bi-TPAI concentration shows stabilized and even slightly increased V_{mpp} over the entire measurement time. Considering that the J_{mpp} for all the samples is stable (**Figure S11**), the V_{mpp} determines the MPPT PCE behavior (**Figure 5b**). This indicates that the amount of cations passivating the perovskite top surface plays a significant role in maintaining the stable operation of the PSCs.[45] In addition, the stability of PSCs is further examed by heating at 85 °C in air with a relative humidity of 10-15%. As shown in **Figure 5c**, after heating for 20 h, the control devices can maintain 87.9% of the initial performance. With the bi-TPAI surface treatment, the devices can maintain >90% of the initial performance, e.g., 94.0% maintained for 0.01 mg/mL bi-TPAI modified PSCs. XRD patterns of the fresh and the aged perovskite films are acquired, and the results are displayed in **Figure 5d**. Notably, there are two additional diffraction peaks located at 11.7° and 12.6° appeared upon aging the control perovskite film, which are attributed to δ-phase perovskite and PbI_2, respectively. Only PbI_2 is observed after aging the bi-TPAI treated perovskite films. δ-phase perovskite is photoinactive, which is reason for the poor stability of the PSCs. The bi-TPAI treatment passivate the surface defects, thus reducing the sites at which perovskite undergoes degradation and improving the stability under moisture and thermal conditions.
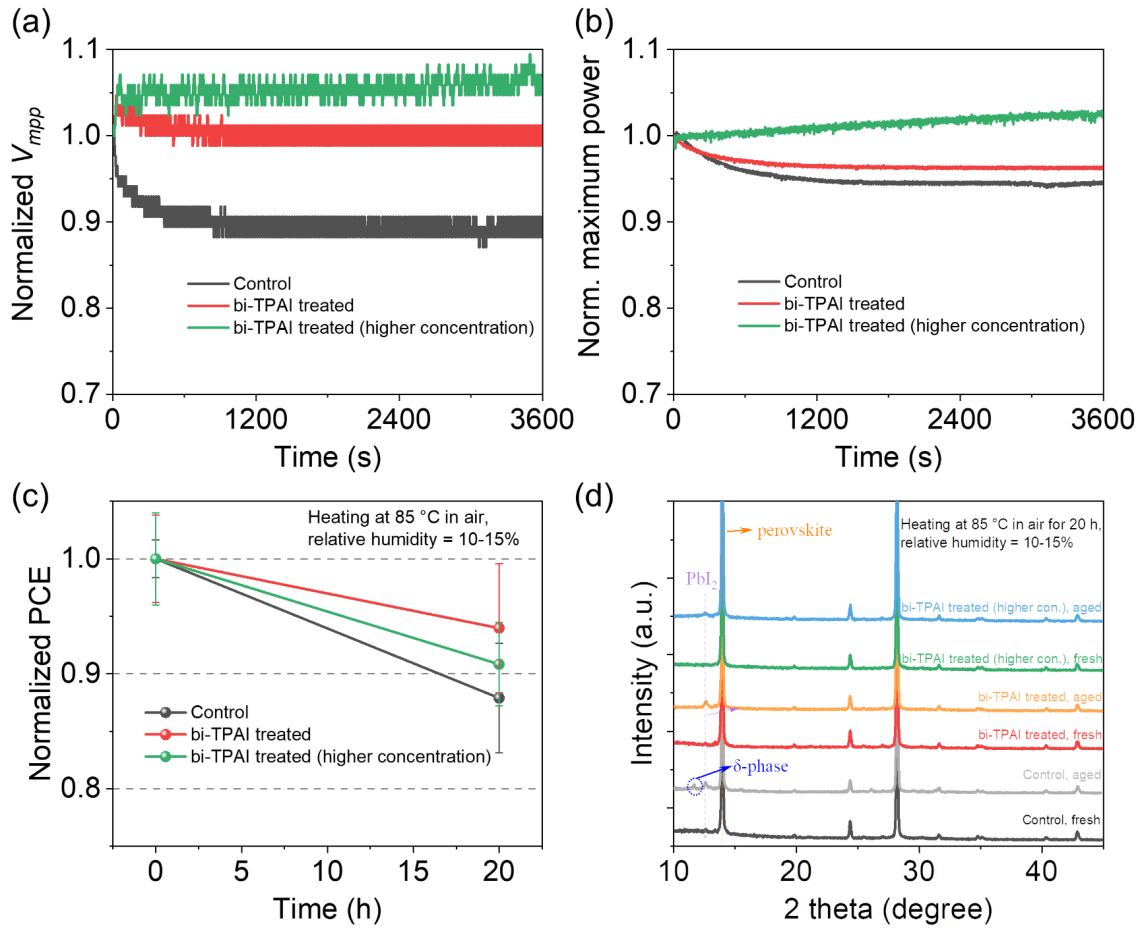
Figure 5. Normalized (a) V_{mpp} and (b) maximum power spectra for the control and the different concentration bi-TPAI treated PSCs during the 1-hour MPPT measurement. (c) Thermal stability of the corresponding PSCs. 9 samples were counted for each condition. (d) XRD patterns of the fresh and aged perovskite films under different conditions.

4. Conclusion

In summary, bi-TPAI has been demonstrated as an effective surface modulator for improving the quality of the perovskite surface. It is found that a moderate amount of bi-TPAI has negligible influence on the surface morphology, optical absorption, and crystal structure of the perovskite films. On the other hand, bi-TPAI treatment can effectively passivate the surface defects, enlarge the V_{bi} and facilitate the charge extraction, contributing to the enhancement of the photovoltaic parameters. Consequently, the best PCE of the corresponding PSCs is improved from the initial 20.0% to 22.0%. Moreover, the burn-in process during MPPT measurements can be largely alleviated or even eliminated by controlling the amount of bi-TPAI, which is related to the fact that bi-TPAI treatment can mitigate the decrease in V_{mpp}. Our work provides new insights to simultaneously improve the initial device efficiency and the operational stability for gas-quenched inverted p-i-n PSCs built on the sputtered NiO_x.

Supporting information

Figures S1–S11 and Table S1-2 as mentioned in the text.

Author contributions

Xin Zhang: conceived the idea, designed the experiments, performed most measurements, and drafted the original manuscript. Stijn Eurelings: fabricated the perovskite solar cells and performed the *J-V* measurements. Andrea Bracesco: carried out XPS measurements. Wenya Song: measured SEM images. Stijn Lenaers: synthesized the bi-TPAI salt. Wouter Van Gompel: supervised Stijn Lenaers and revised the manuscript. Anurag Krishna: revised the manuscript. Tom Aernouts: supervised Xin Zhang. Laurence Lutsen: responsible for funding acquisition and project management. Dirk Vanderzande: supervised Stijn Lenaers. Mariadriana Creatore: contributed to the scientific discussion of the XPS results. Yiqiang Zhan: revised the manuscript. Yinghuan Kuang: supervised Xin Zhang and revised the manuscript. Jef Poortmans: supervised the work, performed project management and provided his expertise.

Conflicts of interest

The authors declare no competing financial interest.

Acknowledgement

References

1.   Tan, Q.; Li, Z.; Luo, G.; Zhang, X.; Che, B.; Chen, G.; Gao, H.; He, D.; Ma, G.; Wang, J.; Xiu, J.; Yi, H.; Chen, T.;He, Z., Inverted perovskite solar cells using dimethylacridine-based dopants. *Nature* **2023**, https://doi.org/10.1038/s41586-023-06207-0.
2.   Saliba, M.; Matsui, T.; Seo, J.-Y.; Domanski, K.; Correa-Baena, J.-P.; Nazeeruddin, M. K.; Zakeeruddin, S. M.; Tress, W.; Abate, A.; Hagfeldt, A.;Grätzel, M., Cesium-containing triple cation perovskite solar cells: improved stability, reproducibility and high efficiency. *Energy & Environmental Science* **2016**, *9* (6), 1989-1997.
3.   Turren-Cruz, S.-H.; Hagfeldt, A.;Saliba, M., Methylammonium-free, high-performance, and stable perovskite solar cells on a planar architecture. *Science* **2018**, *362* (6413), 449-453.
4.   Li, S.; Zhu, L.; Kan, Z.; Hua, Y.;Wu, F., A multifunctional additive of scandium trifluoromethanesulfonate to achieve efficient inverted perovskite solar cells with a high fill factor of 83.80%. *Journal of Materials Chemistry A* **2020,** *8* (37), 19555-19560.
5.   Bu, T.; Liu, X.; Zhou, Y.; Yi, J.; Huang, X.; Luo, L.; Xiao, J.; Ku, Z.; Peng, Y.; Huang, F.; Cheng, Y.-B.;Zhong, J., A novel quadruple-cation absorber for universal hysteresis elimination for high efficiency and stable perovskite solar cells. *Energy & Environmental Science* **2017,** *10* (12), 2509-2515.
6.   Chen, K.; Lu, H.; Yang, Y.; Li, S.; Jia, K.; Wu, F.;Zhu, L., Simultaneously Modifying Hole Transport Material and Perovskite via a Crown Ether-Based Semiconductor Toward Efficient and Stable Perovskite Solar Cells. *Solar RRL* **2023,** *7* (4), 2200987.
7.   Gao, X.-X.; Ding, B.; Kanda, H.; Fei, Z.; Luo, W.; Zhang, Y.; Shibayama, N.; Züttel, A.; Tirani, F. F.; Scopelliti, R.; Kinge, S.; Zhang, B.; Feng, Y.; Dyson, P. J.;Nazeeruddin, M. K., Engineering long-term stability into perovskite solar cells via application of a multi-functional TFSI-based ionic liquid. *Cell Reports Physical Science* **2021,** *2* (7), 100475.
8.   Kim, W.; Park, J. B.; Kim, H.; Kim, K.; Park, J.; Cho, S.; Lee, H.; Pak, Y.;Jung, G. Y., Enhanced long-term stability of perovskite solar cells by passivating grain boundary with polydimethylsiloxane (PDMS). *Journal of Materials Chemistry A* **2019,** *7* (36), 20832-20839.
9.   Bai, S.; Da, P.; Li, C.; Wang, Z.; Yuan, Z.; Fu, F.; Kawecki, M.; Liu, X.; Sakai, N.; Wang, J. T.-W.; Huettner, S.; Buecheler, S.; Fahlman, M.; Gao, F.;Snaith, H. J., Planar perovskite solar cells with long-term stability using ionic liquid additives. *Nature* **2019,** *571* (7764), 245-250.
10.   Koh, C. W.; Heo, J. H.; Uddin, M. A.; Kwon, Y.-W.; Choi, D. H.; Im, S. H.;Woo, H. Y., Enhanced Efficiency and Long-Term Stability of Perovskite Solar Cells by Synergistic Effect of Nonhygroscopic Doping in Conjugated Polymer-Based Hole-Transporting Layer. *ACS Applied Materials & Interfaces* **2017,** *9* (50), 43846-43854.
11.   Chen, C.; Li, H.; Jin, J.; Cheng, Y.; Liu, D.; Song, H.;Dai, Q., Highly enhanced long time stability of perovskite solar cells by involving a hydrophobic hole modification layer. *Nano Energy* **2017,** *32*, 165-173.
12.   Liao, Q.; Wang, Y.; Yao, X.; Su, M.; Li, B.; Sun, H.; Huang, J.;Guo, X., A Dual-Functional Conjugated Polymer as an Efficient Hole-Transporting Layer for High-Performance Inverted Perovskite Solar Cells. *ACS Applied Materials & Interfaces* **2021,** *13* (14), 16744-16753.
13.   Kong, W.; Li, W.; Liu, C.; Liu, H.; Miao, J.; Wang, W.; Chen, S.; Hu, M.; Li, D.; Amini, A.; Yang, S.; Wang, J.; Xu, B.;Cheng, C., Organic Monomolecular Layers Enable Energy-

Level Matching for Efficient Hole Transporting Layer Free Inverted Perovskite Solar Cells. *ACS Nano* **2019,** *13* (2), 1625-1634.

14.   Li, B.; Yang, K.; Liao, Q.; Wang, Y.; Su, M.; Li, Y.; Shi, Y.; Feng, X.; Huang, J.; Sun, H.;Guo, X., Imide-Functionalized Triarylamine-Based Donor-Acceptor Polymers as Hole Transporting Layers for High-Performance Inverted Perovskite Solar Cells. *Advanced Functional Materials* **2021,** *31* (21), 2100332.

15.   Yang, D.; Sano, T.; Yaguchi, Y.; Sun, H.; Sasabe, H.;Kido, J., Achieving 20% Efficiency for Low-Temperature-Processed Inverted Perovskite Solar Cells. *Advanced Functional Materials* **2019,** *29* (12), 1807556.

16.   Lammar, S.; Van Gompel, W.; Lenaers, S.; Mertens, M.; Boyen, H.-G.; Desta, D.; Hadipour, A.; Lutsen, L.; Vanderzande, D.; Krishna, A.; Abdulraheem, Y.; Aernouts, T.;Poortmans, J., Organic ammonium iodide salts as passivation for buried interface enables efficient and stable NiO_x based p-i-n perovskite solar cells. *Journal of Materials Chemistry C* **2023,** *11*, 8146-8153.

17.   Chen, Y.; Yang, Z.; Jia, X.; Wu, Y.; Yuan, N.; Ding, J.; Zhang, W.-H.;Liu, S., Thermally stable methylammonium-free inverted perovskite solar cells with Zn^{2+} doped CuGaO2 as efficient mesoporous hole-transporting layer. *Nano Energy* **2019,** *61*, 148-157.

18.   Arumugam, G. M.; Karunakaran, S. K.; Liu, C.; Zhang, C.; Guo, F.; Wu, S.;Mai, Y., Inorganic hole transport layers in inverted perovskite solar cells: A review. *Nano Select* **2021,** *2* (6), 1081-1116.

19.   Sun, W.; Li, Y.; Ye, S.; Rao, H.; Yan, W.; Peng, H.; Li, Y.; Liu, Z.; Wang, S.; Chen, Z.; Xiao, L.; Bian, Z.;Huang, C., High-performance inverted planar heterojunction perovskite solar cells based on a solution-processed CuO_x hole transport layer. *Nanoscale* **2016,** *8* (20), 10806-10813.

20.   Li, Z.; Li, B.; Wu, X.; Sheppard, S. A.; Zhang, S.; Gao, D.; Long, N. J.;Zhu, Z., Organometallic-functionalized interfaces for highly efficient inverted perovskite solar cells. *Science* **2022,** *376* (6591), 416-420.

21.   Boyd, C. C.; Shallcross, R. C.; Moot, T.; Kerner, R.; Bertoluzzi, L.; Onno, A.; Kavadiya, S.; Chosy, C.; Wolf, E. J.; Werner, J.; Raiford, J. A.; de Paula, C.; Palmstrom, A. F.; Yu, Z. J.; Berry, J. J.; Bent, S. F.; Holman, Z. C.; Luther, J. M.; Ratcliff, E. L.; Armstrong, N. R.;McGehee, M. D., Overcoming Redox Reactions at Perovskite-Nickel Oxide Interfaces to Boost Voltages in Perovskite Solar Cells. *Joule* **2020,** *4* (8), 1759-1775.

22.   Li, L.; Wang, Y.; Wang, X.; Lin, R.; Luo, X.; Liu, Z.; Zhou, K.; Xiong, S.; Bao, Q.; Chen, G.; Tian, Y.; Deng, Y.; Xiao, K.; Wu, J.; Saidaminov, M. I.; Lin, H.; Ma, C.-Q.; Zhao, Z.; Wu, Y.; Zhang, L.;Tan, H., Flexible all-perovskite tandem solar cells approaching 25% efficiency with molecule-bridged hole-selective contact. *Nature Energy* **2022,** *7* (8), 708-717.

23.   Mann, D. S.; Patil, P.; Kwon, S.-N.;Na, S.-I., Enhanced performance of p-i-n perovskite solar cell via defect passivation of nickel oxide/perovskite interface with self-assembled monolayer. *Applied Surface Science* **2021,** *560*, 149973.

24.   Guo, T.; Fang, Z.; Zhang, Z.; Deng, Z.; Zhao, R.; Zhang, J.; Shang, M.; Liu, X.; Hu, Z.; Zhu, Y.;Han, L., Self-assembled interlayer aiming at the stability of NiOx based perovskite solar cells. *Journal of Energy Chemistry* **2022,** *69*, 211-220.

25.   Hang, P.; Xie, J.; Kan, C.; Li, B.; Zhang, Y.; Gao, P.; Yang, D.;Yu, X., Stabilizing Fullerene for Burn-in-Free and Stable Perovskite Solar Cells under Ultraviolet Preconditioning and Light Soaking. *Advanced Materials* **2021,** *33* (10), 2006910.

26.   Paek, S.; Khan, S. B.; Franckevičius, M.; Gegevičius, R.; A. Syzgantseva, O.; Syzgantseva, M. A.; Kinche, S.; Asiri, A. M.; Roldán-Carmona, C.;Nazeeruddin, M. K., Cation optimization for burn-in loss-free perovskite solar devices. *Journal of Materials Chemistry A* **2021,** *9* (9), 5374-5380.

27. Domanski, K.; Roose, B.; Matsui, T.; Saliba, M.; Turren-Cruz, S.-H.; Correa-Baena, J.-P.; Carmona, C. R.; Richardson, G.; Foster, J. M.; De Angelis, F.; Ball, J. M.; Petrozza, A.; Mine, N.; Nazeeruddin, M. K.; Tress, W.; Grätzel, M.; Steiner, U.; Hagfeldt, A.;Abate, A., Migration of cations induces reversible performance losses over day/night cycling in perovskite solar cells. *Energy & Environmental Science* **2017,** *10* (2), 604-613.

28. Zhang, Z.; Qiao, L.; Meng, K.; Long, R.; Chen, G.;Gao, P., Rationalization of passivation strategies toward high-performance perovskite solar cells. *Chemical Society Reviews* **2023,** *52* (1), 163-195.

29. Jiang, Q.; Tong, J.; Xian, Y.; Kerner, R. A.; Dunfield, S. P.; Xiao, C.; Scheidt, R. A.; Kuciauskas, D.; Wang, X.; Hautzinger, M. P.; Tirawat, R.; Beard, M. C.; Fenning, D. P.; Berry, J. J.; Larson, B. W.; Yan, Y.;Zhu, K., Surface reaction for efficient and stable inverted perovskite solar cells. *Nature* **2022,** *611* (7935), 278-283.

30. Zhang, W.; Shen, H.; Yan, P.;Zhang, J., Interfacial engineering of sputtered NiOx for enhancing efficiency and stability of inverted perovskite solar cells. *Solar Energy* **2022,** *248*, 128-136.

31. Zheng, X.; Song, Z.; Chen, Z.; Bista, S. S.; Gui, P.; Shrestha, N.; Chen, C.; Li, C.; Yin, X.; Awni, R. A.; Lei, H.; Tao, C.; Ellingson, R. J.; Yan, Y.;Fang, G., Interface modification of sputtered NiOx as the hole-transporting layer for efficient inverted planar perovskite solar cells. *Journal of Materials Chemistry C* **2020,** *8* (6), 1972-1980.

32. Lammar, S.; Van Gompel, W.; Lenaers, S.; Mertens, M.; Boyen, H.-G.; Desta, D.; Hadipour, A.; Lutsen, L.; Vanderzande, D.; Krishna, A.; Abdulraheem, Y.; Aernouts, T.;Poortmans, J., Organic ammonium iodide salts as passivation for buried interface enables efficient and stable NiO$_x$ based p-i-n perovskite solar cells. *Journal of Materials Chemistry C* **2023**, 8146-8153.

33. Peng, Z.; Zuo, Z.; Qi, Q.; Hou, S.; Fu, Y.;Zou, D., Managing the Double-Edged Sword of Ni^{3+} in Sputter-Deposited NiOx by Interfacial Redox Reactions for Efficient Perovskite Solar Cells. *ACS Applied Energy Materials* **2023,** *6* (3), 1396-1403.

34. Itzhak, A.; He, X.; Kama, A.; Kumar, S.; Ejgenberg, M.; Kahn, A.;Cahen, D., NiN-Passivated NiO Hole-Transport Layer Improves Halide Perovskite-Based Solar Cell. *ACS Appl Mater Interfaces* **2022,** *14* (42), 47587-47594.

35. Denis, P.-H.; Mertens, M.; Van Gompel, W. T. M.; Van Hecke, K.; Ruttens, B.; D'Haen, J.; Lutsen, L.;Vanderzande, D., Directing the Self-Assembly of Conjugated Organic Ammonium Cations in Low-Dimensional Perovskites by Halide Substitution. *Chemistry of Materials* **2021,** *33* (13), 5177-5188.

36. Rakocevic, L.; Ernst, F.; Yimga, N. T.; Vashishtha, S.; Aernouts, T.; Heumueller, T.; Brabec, C. J.; Gehlhaar, R.;Poortmans, J., Reliable Performance Comparison of Perovskite Solar Cells Using Optimized Maximum Power Point Tracking. *Solar RRL* **2019,** *3* (2), 1800287.

37. Zhou, Q.; Liang, L.; Hu, J.; Cao, B.; Yang, L.; Wu, T.; Li, X.; Zhang, B.;Gao, P., High-Performance Perovskite Solar Cells with Enhanced Environmental Stability Based on a (p-FC6H4C2H4NH3)2[PbI4] Capping Layer. *Advanced Energy Materials* **2019,** *9* (12), 1802595.

38. Zhou, N.; Shen, Y.; Zhang, Y.; Xu, Z.; Zheng, G.; Li, L.; Chen, Q.;Zhou, H., CsI Pre-Intercalation in the Inorganic Framework for Efficient and Stable FA$_{1-x}$Cs$_x$PbI$_3$(Cl) Perovskite Solar Cells. *Small* **2017,** *13* (23), 1700484.

39. Cao, Q.; Li, Y.; Zhang, H.; Yang, J.; Han, J.; Xu, T.; Wang, S.; Wang, Z.; Gao, B.; Zhao, J.; Li, X.; Ma, X.; Zakeeruddin, S. M.; Sha, W. E. I.; Li, X.;Grätzel, M., Efficient and stable inverted perovskite solar cells with very high fill factors via incorporation of star-shaped polymer. *Science advances* **2021,** *7* (28), eabg0633.

40. Xiong, S.; Hou, Z.; Zou, S.; Lu, X.; Yang, J.; Hao, T.; Zhou, Z.; Xu, J.; Zeng, Y.; Xiao, W.; Dong, W.; Li, D.; Wang, X.; Hu, Z.; Sun, L.; Wu, Y.; Liu, X.; Ding, L.; Sun, Z.; Fahlman,

M.;Bao, Q., Direct Observation on p- to n-Type Transformation of Perovskite Surface Region during Defect Passivation Driving High Photovoltaic Efficiency. *Joule* **2021,** *5* (2), 467-480.

41. Xiang, S.; Li, W.; Wei, Y.; Liu, J.; Liu, H.; Zhu, L.; Yang, S.;Chen, H., Natrium Doping Pushes the Efficiency of Carbon-Based $CsPbI_3$ Perovskite Solar Cells to 10.7%. *iScience* **2019,** *15*, 156-164.

42. Li, X.; Zhang, W.; Guo, X.; Lu, C.; Wei, J.;Fang, J. J. S., Constructing heterojunctions by surface sulfidation for efficient inverted perovskite solar cells. *Science* **2022,** *375*, 434 - 437.

43. Meng, L.; Sun, C.; Wang, R.; Huang, W.; Zhao, Z.; Sun, P.; Huang, T.; Xue, J.; Lee, J. W.; Zhu, C.; Huang, Y.; Li, Y.;Yang, Y., Tailored Phase Conversion under Conjugated Polymer Enables Thermally Stable Perovskite Solar Cells with Efficiency Exceeding 21%. *Journal of the American Chemical Society* **2018,** *140* (49), 17255-17262.

44. Azmi, R.; Ugur, E.; Seitkhan, A.; Aljamaan, F.; Subbiah, A. S.; Liu, J.; Harrison, G. T.; Nugraha, M. I.; Eswaran, M. K.; Babics, M.; Chen, Y.; Xu, F.; Allen, T. G.; Rehman, A. U.; Wang, C. L.; Anthopoulos, T. D.; Schwingenschlögl, U.; De Bastiani, M.; Aydin, E.;De Wolf, S., Damp heat-stable perovskite solar cells with tailored-dimensionality 2D/3D heterojunctions. *Science* **2022,** *376* (6588), 73-77.

45. Song, W.; Zhang, X.; Lammar, S.; Qiu, W.; Kuang, Y.; Ruttens, B.; D'Haen, J.; Vaesen, I.; Conard, T.; Abdulraheem, Y.; Aernouts, T.; Zhan, Y.;Poortmans, J., Critical Role of Perovskite Film Stoichiometry in Determining Solar Cell Operational Stability: a Study on the Effects of Volatile A-Cation Additives. *ACS Applied Materials & Interfaces* **2022,** *14* (24), 27922-27931.

Table of content: